



Catalytic activity for direct CO₂ hydrogenation to dimethyl ether with different proximity of bifunctional Cu-ZnO-Al₂O₃ and ferrierite

Xu Wang¹, So Yun Jeong¹, Hyun Seung Jung, Dongming Shen, Mansoor Ali, Faisal Zafar, Chan-Hwa Chung, Jong Wook Bae^{*}

School of Chemical Engineering, Sungkyunkwan University (SKKU), 2066 Seobu-ro, Jangnan-gu, Suwon, Gyeonggi-do 16419, Republic of Korea

ARTICLE INFO

Keywords:

CO₂ hydrogenation
Dimethyl ether (DME)
Close proximity
Migration of metal ions
Stability of Cu nanoparticles

ABSTRACT

Dimethyl ether (DME) can be directly synthesized by carbon dioxide (CO₂) hydrogenation over bifunctional catalysts, which are suffered from various deactivation mechanisms caused by incompatible integrations of metal oxides and solid acid zeolites according to their different proximity. The core-shell structured integrations of Cu-ZnO-Al₂O₃ metal oxide (CZA) and ferrierite zeolite (FER) are investigated for direct CO₂ hydrogenation to DME. The detrimental and undesired surface properties formed by a possible ion-exchange of FER surfaces with the relatively volatile metal ions from Cu-ZnO-Al₂O₃ surfaces were effectively suppressed by applying the physically-coated interlayers with SiO₂ (CZA@FER) compared to the powder-mixed one (CZA/FER), where an intimate proximity of metal oxides and FER was eventually responsible for an increased CO selectivity and deactivation rate. The SiO₂ interlayers to isolate the CZA and FER with a suppressed migration of metal ions to FER surfaces further stabilized the active Cu-ZnO nanoparticles and acidic sites of FER surfaces.

1. Introduction

The recent highly required energy supplements have been responsible for a huge amount of carbon dioxide (CO₂) emission, which leads detrimental environmental concerns such as global warming problems. Various chemical utilizations of CO₂ to the value-added petrochemicals provide the most promising approaches to cut down CO₂ emission. Among the petrochemicals, dimethyl ether (DME), as one of alternative clean fuels with higher cetane value and important platform intermediate to produce value-added chemicals through C₁ chemistry, can be directly synthesized by catalytic CO₂ hydrogenation over various bifunctional catalysts, which can be integrated with consecutive two step reactions such as CO₂ hydrogenation to methanol (CO₂ + 3 H₂ → CH₃OH + H₂O, ΔH_{298 K} = −49.4 kJ/mol) and successive dehydration to DME (2CH₃OH → CH₃OCH₃ + H₂O, ΔH_{298 K} = −23.4 kJ/mol) with its much thermodynamically feasible reaction (2CO₂ + 6 H₂ → CH₃OCH₃ + 3 H₂O, ΔH_{298 K} = −122.2 kJ/mol) [1–3]. For the tandem reaction, a reverse water gas shift (RWGS) reaction inevitably occurs as one of the main side reactions to form CO (CO₂ + H₂ ⇌ CO + H₂O), and the bifunctional catalysts containing Cu-ZnO-Al₂O₃ (CZA) or Cu-Zn-ZrO₂ as methanol synthesis component [4–8] can be generally hybridized with

various solid acid zeolites having different topologies such as MFI, FER, BEA or MOR as methanol dehydration component for the direct DME synthesis by CO_x (CO/CO₂) hydrogenation [4,5]. Among the well-known zeolites, FER zeolite has been proposed as one of the excellent candidates for methanol dehydration to DME due to its beneficial 2-D topology natures with fast diffusion rate, less formation of cokes and suitable acidic properties [9,10].

To synthesize those effective bifunctional catalysts, the most prevailing approach is to use a physical powder-mixing method due to its simplest procedure and weak interactions between metal oxides and solid acid zeolites [11–13]. Generally, the proximity-dependence of two active components can largely change catalytic stability and product selectivity [14–17], and their closer interactions seem to be intrinsically beneficial in terms of fast diffusion rate as well as fast transformation rate of surface intermediates [14]. However, it was found that the closer proximity of two active components on the bifunctional catalysts was detrimental for catalytic performances such as lower yield to desired products [15], where the significant progresses for the tandem catalytic reactions with the hybridized metal oxides and zeolites have been achieved in the field of C₁ chemistry for CO_x hydrogenations [16–20]. According to different proximity for some distinctive catalytic reactions,

^{*} Corresponding author.

E-mail address: finejw@skku.edu (J.W. Bae).

¹ X. Wang and S.Y. Jeong contributed equally.

large changes of product distributions and catalytic stability have been reported, which were possibly caused by the altered reaction-diffusion dynamics as well [16–19,21]. In addition, some adverse effects such as metal ion-exchange-induced zeolite modifications as well as concomitant-induced side reactions have been reported when two components are closely contacted with an intimate proximity [22–24]. For example, the CZA metal oxides integrated with FER zeolite can be suffered from individual deactivation phenomena, which can be caused by an incompatibility of CZA and FER component in their intimate proximity with stepwise changes of catalytic stability and selectivity for a direct CO₂ hydrogenation to DME [25,26]. In addition, the intimate proximity of Cu and Zn metal ions on the CZA metal oxides can be generally responsible for its higher mobility with the help of the formed water during CO₂ hydrogenation reaction, which can enhance an ion-exchange-reaction between CZA and zeolite by neutralizing the active Brønsted acid sites of zeolite for methanol dehydration with its successive deactivation [27].

To overcome those drawbacks for direct CO₂ hydrogenation to DME with a proper proximity between CZA and FER component, the synergy effects with SiO₂ interlayer coating method between CZA and FER can be realized to suppress Cu/Zn ion migrations and to isolate CZA and FER with micrometer scale proximity. In addition, the core-shell structured CZA@FER prepared by a physically coating method with SiO₂ interlayer was investigated by varying the proximity scale to verify the relationships between the proximity, catalytic activity and stability.

2. Experimental section

2.1. Catalyst preparation and activity evaluation

The physically powder-mixed bifunctional CZA/FER catalyst was prepared by a simple physical mixing method through a mortar grinding method to obtain well-mixed bifunctional catalyst. Previously, separate CZA and FER component were respectively synthesized by a co-precipitation and hydrothermal synthesis according to our previous work [6]. For CZA preparation, Cu/Zn/Al metal nitrate precursors with their molar ratio of Cu/Zn/Al = 1/0.43/0.28 (corresponding to CuO/ZnO/Al₂O₃ molar ratio = 7:3:1) and ammonium carbonate precipitation agent were used to prepare the CZA precipitates, which was calcined at 350 °C for 2 h. For the synthesis of FER zeolite, Na-form FER was previously synthesized and followed by an ion-exchange step to obtain H-form FER having a Si/Al molar ratio of 11.7 (confirmed by XRF analysis) followed by calcining at 550 °C for 3 h. Finally, the CZA and FER powder was thoroughly mixed by using a mortar grinding with its weight ratio of 10–2 (CZA to FER) for the preparation of the physically powder-mixed bifunctional CZA/FER catalyst.

The core-shell structured CZA@FER catalyst was prepared according to the previous report [28] by using additional SiO₂ coating interlayers. For more details, as-prepared CZA powder was pelletized, crushed and sieved in the range of 600–710 μm. The dispersed 0.2 g silica sol (Ludox, 40 wt%, Aldrich) in 0.6 g deionized water (DIW) was previously prepared as an adhesive material, and 1.0 g of the CZA as a core part was soaked in the diluted silica sol for 10 min and filtered. Successively, the collected wet CZA powder in a round bottom flask was mixed with a fixed amount of FER under a vigorous shaking condition until the FER shell side was totally adhered on the external surfaces of the granule-type CZA core part, which was previously coated with SiO₂ interlayers. Repeating those procedures several times until total amount of CZA to FER of 10–2 (weight ratio), and the final resultants were dried at 80 °C at a convection oven overnight, and it was calcined at 500 °C for 2 h at much higher temperature than the CZA component to stabilize the SiO₂ interlayer coating material. In addition, the reference Cu or Zn-modified FER zeolite (Cu-FER, Zn-FER) were separately prepared by an impregnation method for XPS analysis. The FER zeolite of 1.0 g was immersed at 80 °C in 100 mL solution containing the separate 1.0 molar Cu or Zn nitrate precursor under vigorous stirring condition for 3 h. The

impregnated catalyst was further filtered and washed with DIW several times followed by drying at 80 °C overnight, and it was calcined at 500 °C for 3 h at a ramp rate of 1 °C/min.

Catalytic activity for the direct CO₂ hydrogenation to DME was evaluated with 0.4 g catalyst, which was previously loaded in a fixed-bed tubular reactor with an inner diameter of 6 mm and length of 453 mm. Prior to the reaction, the catalyst was reduced at 300 °C for 5 h under a flow of 5 vol% H₂ balanced with N₂. The mixed gas with a molar ratio of CO₂/H₂/N₂ = 72/24/4 (N₂ as an internal standard gas and H₂/CO₂ = 3) at a weight hourly space velocity (SV) = 5000 mL/(g_{cat}·h) was used for CO₂ hydrogenation at a fixed reaction pressure of 5.0 MPa. After increasing the reaction pressure up to 5.0 MPa, reaction temperature was increased up to 260 °C and kept for 40 h of reaction duration, and the effluent gases were simultaneously analyzed by using a gas chromatography (GC, YL6100, Younglin). The GC was equipped with a thermal conductivity detector (TCD) and flame ionization detector (FID) connected to separate column such as a Carboxen-1000 packed column for TCD to analyze non-flammable gases and DB-Wax-UI capillary column for FID to analyze oxygenates and hydrocarbons. Conversion of CO₂ ($X_{CO_2} = (1 - N_{i,out}/N_{i,in}) \times 100\%$) and selectivity of products ($S_j = (N_j/(N_{i,in} - N_{i,out})) \times 100\%$) with a unit of mol% based on total carbon mol balance were calculated, where N stands for an inlet and outlet mols of CO₂ reactant and products such as DME, methanol, and hydrocarbons.

2.2. Catalyst characterization

Textual properties such as specific surface area (S_g , m²/g), pore volume (P_v , cm³/g) and average pore diameter (P_D , nm) of the fresh bifunctional CZA-FER catalysts (CZA/FER and CZA@FER) were determined by N₂ adsorption-desorption analysis with a TRISTAR-3000 instrument (Micromeritics) at a liquid N₂ temperature of –196 °C. Multipoint Brunauer-Emmett-Teller (BET) method was applied to calculate specific surface area by using the data in the P/P_0 range of 0.03–0.2. Pore volume was collected at a relative pressure of 0.99 and average pore diameter and pore size distribution were obtained with the help of Barrett-Joyner-Halenda (BJH) method from the desorption branch of N₂-sorption isotherm. Powder X-ray diffraction (XRD) patterns for the fresh, reduced and used CZA-FER catalysts were obtained to verify the crystalline phases of Cu species and FER zeolite in the range of 5–90° by using a X'Pert PRO MPD diffractometer (Malvern Panalytical) installed with a Cu Kα radiation. The crystallite sizes of the separate Cu species such as metallic Cu and CuO were calculated with the help of Scherrer equation by using the most intensive characteristic diffraction peaks.

The reduction behaviors of the fresh CZA-FER bifunctional catalysts were verified by a temperature-programmed reduction with H₂ (TPR) by using 5 vol% H₂ balanced with Ar with a BELCAT-M instrument. Prior to the analysis, the fresh sample with 50 mg was loaded in a TPR cell and purged at 300 °C for 3 h at a ramping rate of 10 °C/min under Ar flow (50 mL/min). The mixed reduction gas (30 mL/min) was switched on the pretreated sample after cooling it down to 50 °C. The reduction patterns of the fresh catalyst in the temperature range of 100–500 °C were collected by using a TCD analyzer after passing the effluent gases over water trap, and the consumed amount of H₂ was also calculated with the unit of mmolH₂/g_{cat}.

Temperature-programmed desorption of NH₃ (NH₃-TPD) analysis on the fresh and used CZA-FER catalysts was carried out by using a BELCAT-M instrument to verify the surface acidic amounts and its strengths. Prior to the analysis, the sample was reduced under a flow 5 vol% H₂ balanced with N₂ at 300 °C for 3 h and purged under He flow to remove physically adsorbed hydrogen for 1 h. The sample was cooled down to 100 °C and NH₃ probe molecule was successively introduced for 1 h to the sample, followed by carrying out the desorption of NH₃ at the temperature range of 100–800 °C with a ramping rate of 10 °C/min, and the desorbed amount of NH₃ were collected by using a TCD analyzer. For the NH₃-TPD on the used catalysts, all steps were carried out with same

procedures except for the pretreatment conditions such as He gas treatment to remove surface impurities at 300 °C for 1 h without additional reduction step. Similar with the NH₃-TPD analysis, temperature-programmed desorption of CO₂ (CO₂-TPD) analysis was carried out to measure the amounts of surface basic sites and its strengths. Before the analysis, the fresh sample with 50 mg was reduced at 300 °C for 1 h and then purged with He gas to remove surface contaminants followed by proceeding CO₂ adsorption at 50 °C for 1 h. And the temperature was increased from 50 to 800 °C at a ramping rate of 10 °C/min and the desorbed amounts of CO₂ were collected with a TCD analyzer as well.

The outermost surface properties such as the metal distribution and oxidation state with their interactions on the fresh and used bifunctional CZA-FER catalysts and Cu or Zn-modified FER (Cu-FER or Zn-FER) were separately measured by using an X-ray photoelectron spectroscopy (XPS) analysis as well as Auger electron spectroscopy (AES) with a PHI Quantera II (Scanning X-Ray Microprobe) instrument equipped with Al K α radiation with an energy of 1484.6 eV at chamber working pressure of 5.0×10^{-7} Pa. Finally, the Cu 2p and Zn 2p peaks were analyzed with a resolution of 0.05 eV to elucidate the changes of binding energy (BE) and Zn/Cu surface atomic ratio after correcting their BEs by using a reference BE of C 1 s of 284.8 eV. In addition, the local surface morphology on the fresh CZA/FER and CZA@FER was also confirmed by using a scanning electron microscopy (SEM) as well as energy dispersive spectrometer (EDS) mapping analysis to verify the surface metal dispersions, where SEM analysis was performed by using a Talos F200S instrument equipped with a field emission gun operated at 200 kV.

3. Results and discussion

3.1. Structural properties of Cu-ZnO-Al₂O₃ incorporated with FER zeolite

Textual properties of the fresh CZA/FER and CZA@FER are summarized in Table 1 and supplementary Table S1, and the specific surface area was found to be much larger on the CZA@FER with 133.2 m²/g compared to that of 58.7 m²/g on the coprecipitated CZA, which was attributed to the presence of FER zeolite having a larger surface area of 424.2 m²/g and the contribution of the mesoporous SiO₂ coating interlayers. The physically powder-mixed CZA/FER exhibited a small

surface area of 93.5 m²/g compared to the SiO₂ interlayer-coated CZA@FER, which can be mainly attributed to the wide range of larger intra-particle pore size distributions on the CZA/FER with much larger pore sizes. The observation was attributed to the presence of heterogeneous size distribution of CZA particles, which was confirmed by wider pore size distribution as well as by much larger average pore diameter of 21.7 nm than that of 9.9 nm on the CZA@FER as displayed in supplementary Fig. S1 even though all catalysts showed very similar micropore and mesopore structures as displayed in Fig. 1(A). The smaller and similar pore volumes on the CZA, CZA/FER and CZA@FER in the range of 0.30 – 0.34 cm³/g than the value of 0.96 cm³/g on the FER itself can be also attributed to the natures of larger mesopores of heterogeneously distributed dominant CZA component.

The crystalline phases of Cu and Zn species and their size variations on the fresh, reduced and used bifunctional CZA-FER catalysts were measured by XRD analysis and the results are displayed in Fig. 1(B) and summarized in Table 1 as well as in supplementary Table S1. On the fresh catalysts, the main CuO phases were clearly observed on the CZA/FER and CZA@FER without any clear peaks assigned to ZnO and Al₂O₃ phases due to their highly-dispersed natures or intrinsically amorphous characteristics [11,29] with clear characteristic peaks of FER zeolite as shown in Fig. 1(B-1). The crystallite size of CuO was found to be much larger on the CZA@FER with 10.7 nm compared to those of the CZA (calined at 350 °C for 2 h) and CZA/FER in the range of 9.0 – 9.4 nm, which seems to be mainly attributed to the higher thermal treatment at 500 °C for 2 h to stabilize the SiO₂ interlayer coating material. On the reduced catalysts, the clear metallic Cu and ZnO phases were observed as displayed in Fig. 1(B-2). The crystallite size of metallic Cu was found to be 10.3, 9.7 and 11.7 nm on the CZA, CZA/FER and CZA@FER, respectively, with a little larger ZnO crystallite size with 7.5 nm on the CZA@FER compared to that of ~6.1 nm on the CZA and CZA/FER due to higher calcination temperature of the CZA@FER as well. On the used catalysts, the metallic Cu and ZnO phases with their aggregated crystallite sizes of 13.6–16.2 nm and 7.1 – 9.7 nm on the CZA/FER and CZA@FER as summarized in supplementary Table S1 were clearly observed and additionally detectable ZnCO₃ phases were also observed on the CZA/FER. The ZnCO₃ phases were well known to be less active by introducing negative effects for CO₂ hydrogenation to methanol due to

Table 1
Bulk and surface properties of the bifunctional CZA-FER catalysts.

Notation ^a	N ₂ -sorption ^b			XRD (nm) ^c			H ₂ -TPR ^d	CO ₂ -TPD ^e	NH ₃ -TPD ^f	XPS and AES (reduced/used) ^g	
	S _g (m ² /g)	P _v (cm ³ /g)	P _D (nm)	CuO (fresh)	Cu ⁰ (reduced)	Cu ⁰ (used)	α / β	W/M/S (mmol/g)	W/M/S (T) (mmol/g)	Cu/Zn	Cu ⁺ / (Cu ⁰ + Cu ⁺)
CZA	58.7	0.30	17.7	9.0	10.3	14.1	5.40/ 0.54	0.18/0.06/ 1.04	-	-	-
CZA/FER	93.5	0.34	21.7	9.4	9.7	13.6	4.26/ 0.44	0.11/0.23/ 1.18	0.16/0.17/0.23 (0.56)	1.41/ 1.21	0.87/0.73
CZA@FER	133.2	0.33	9.9	10.7	11.5	16.2	3.97/ 1.47	0.15/0.03/ 0.27	-/0.04/0.04(0.08)	1.08/ 0.83	0.84/0.88

^aCZA and FER represent the Cu-ZnO-Al₂O₃ metal oxides (molar ratio of Cu/ZnAl = 1/0.43/0.28) and ferrierite (FER) zeolite, respectively. CZA/FER stands for the physically powder-mixed catalyst and CZA@FER represents the SiO₂ interlayers-coated core(CZA)-shell(FER) structured catalyst at a fixed CZA to FER weight ratio of 10/2.

^bSpecific surface area (S_g, m²/g), pore volume (P_v, cm³/g) and average pore diameter (P_D, nm) of the fresh bifunctional CZA-FER catalysts were measured by N₂ adsorption-desorption analysis.

^cCrystallite size of CuO and metallic Cu (Cu⁰) was calculated their most intense characteristic XRD peaks by using Scherrer equation on the fresh, reduced and used CZA-FER catalysts, respectively.

^dH₂ consumption at ~280 and ~350 °C (mmolH₂/g_{cat}) from TPR peaks was assigned to the α and β peaks.

^eCO₂-TPD analysis was carried out on the pre-reduced CZA-FER catalysts at 300 °C for 1 h and subsequent CO₂ adsorption at 50 °C for 1 h. Weak (W), medium (M) and strong (S) basic sites were calculated from the peaks appeared at < 250 °C, 250 – 500 °C and > 500 °C, respectively.

^fAmount of surface acidic sites (mmol/g) on the fresh CZA-FER catalysts were calculated by deconvoluting the NH₃-TPD peaks with their characteristic strengths such as weak (W), medium (M) and strong (S) acidic sites with their total acidic sites (T) at the desorption temperature ranges of < 300, 300 – 400 and > 400 °C, respectively. The FER zeolite itself has a specific surface area of 424.2 m²/g (Si/Al ratio of ~12) and their respective surface acid sites of 0.41, 0.13 and 0.17 mmol/g for the W, M and S sites with total sites of 0.71 mmol/g.

^gSurface ratio of Cu/Zn and Cu⁺/(Cu⁰ + Cu⁺) on the reduced and used CZA-FER catalysts were separately analyzed by XPS and AES analysis from the characteristic Cu 2p and Zn 2p peaks.

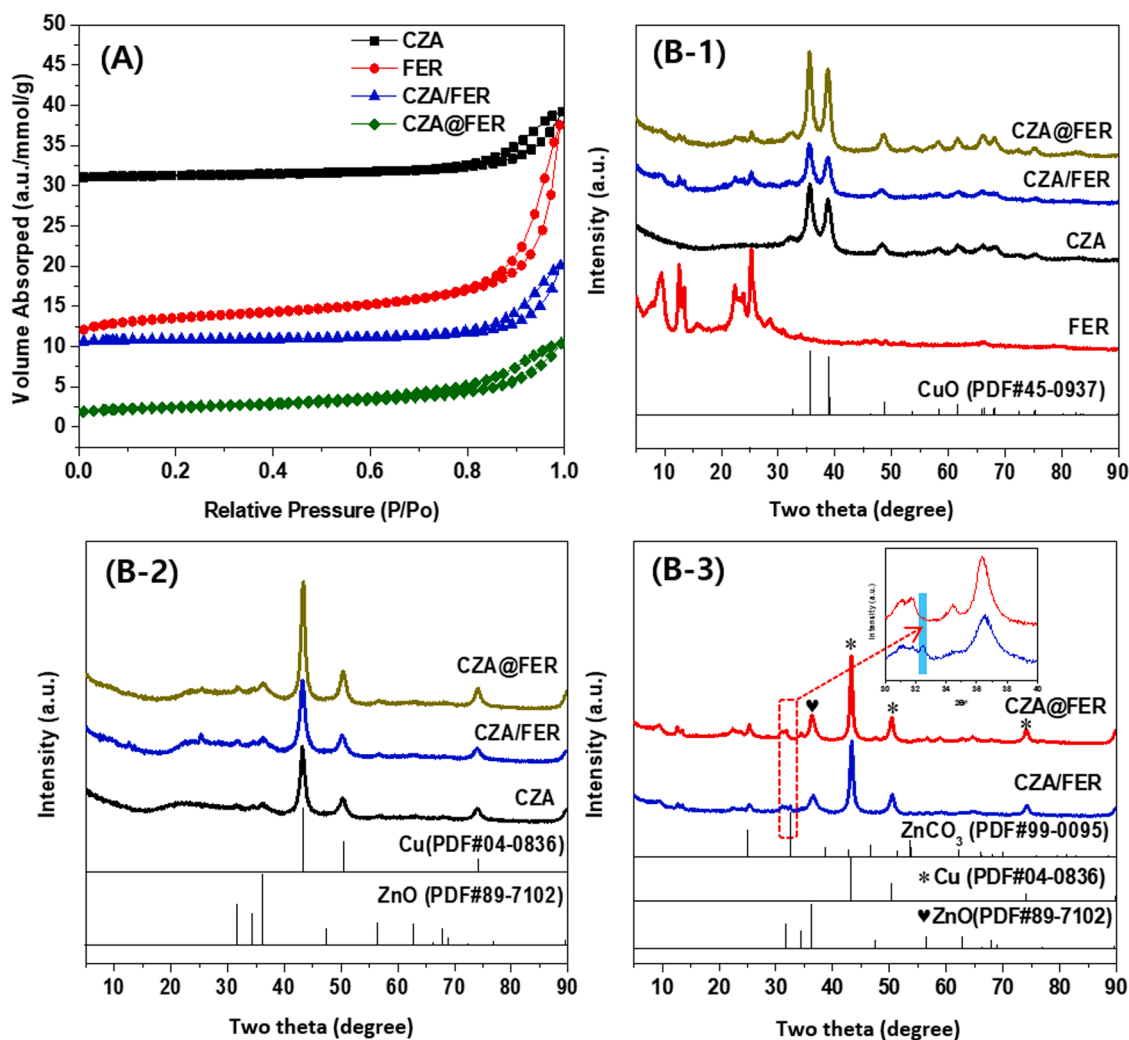


Fig. 1. (A) N₂-sorption patterns on the fresh bifunctional catalysts and (B) XRD patterns of (1) fresh, (2) reduced and (3) used bifunctional CZA-FER catalysts.

an increased RWGS reaction activity to form CO byproduct [30,31]. It is worth to note that the formation of ZnCO₃ phases on the used CZA/FER even with the stable preservation of smaller metallic Cu size can be responsible for the suppressed activity for CO₂ hydrogenation by largely altering product distributions with time on stream, which can be originated from the possible surface rearrangements and phase changes of Cu and ZnO species during the present tandem reaction of direct CO₂ hydrogenation to DME on two active sites.

The local morphology and element distribution on the fresh bifunctional CZA-FER catalysts were measured by SEM and SEM-EDS analysis, and the images are displayed in Fig. 2. The CZA component clearly showed the larger aggregated Cu-ZnO-Al₂O₃ nanoparticles (Fig. 2(A)), and the characteristic nanosheets-like morphology of the FER were also aggregated to form much larger particles (Fig. 2 (B)). The physical powder-mixing step of two compounds on the CZA/FER (Fig. 2 (C)) revealed the randomly distributed smaller CZA nanoparticles on the FER surfaces with a representative close nanometer-scale proximity. Interestingly, the SiO₂-interlayer-coated CZA@FER clearly showed their much larger sizes with a few hundred micrometer-scaled nanoparticles due to the usages of 600–710 μm-sized CZA component (Fig. 2 (D)). It is worth to note that the clear interfaces between the CZA and FER zeolite, where the CZA component was isolated by SiO₂ interlayers with its thickness of ~40 μm coated with the FER layers with 50 μm in thickness as confirmed by SEM-EDS mapping in Figs. 2(E) and 2(F). The observation suggests that the representative micrometer-scale proximity on the CZA@FER, which were responsible for different CO₂ hydrogenation

activity and product distributions as well. In addition, the metal oxides incorporated with zeolites on the bifunctional catalysts can be suffered from the volatile metal migrations, which can detrimentally cause the unexpected product distribution and fast deactivation [22–24]. Those possible migrations of Cu and Zn metal ions during the present tandem reaction were verified by SEM-EDS analysis on the fresh and used CZA/FER and CZA@FER catalysts and the images are displayed in Fig. 3. The distributions of Cu and Zn metals on the physically powder-mixed CZA/FER were found to be well dispersed on the FER surfaces even after the reaction as displayed in Figs. 3(A-1) and 3(A-2), which revealed the nanometer-scale proximity between the CZA and FER species was responsible for an enhanced mobility of metal ions on the outer surfaces of the FER zeolite by subsequently altering the surface acidic natures during catalyst preparation or reaction step. As shown in supplementary Fig. S2, the observed larger amounts of surface Cu and Zn metals on the fresh CZA/FER compared to the fresh CZA@FER with the respective values for Cu metal from 1.97 to 0.23 and Zn metal from 0.52 to 0.18 revealed the highly dispersed Cu/Zn metal ions on the physically power-mixed CZA/FER surfaces. The results also suggest that the profound effects on the catalytic activity and stability of product distribution, which were mainly affected from the very beginning of bifunctional catalyst preparation step. Although the relatively higher migrations of those Cu/Zn metal ions were observed on the used CZA@FER compared to the CZA/FER, the contents of migrated metal ions were still found to be higher on the CZA/FER with the respective values of Cu metal from 1.61 to 0.79 and Zn metal from 0.43 to 0.49. As

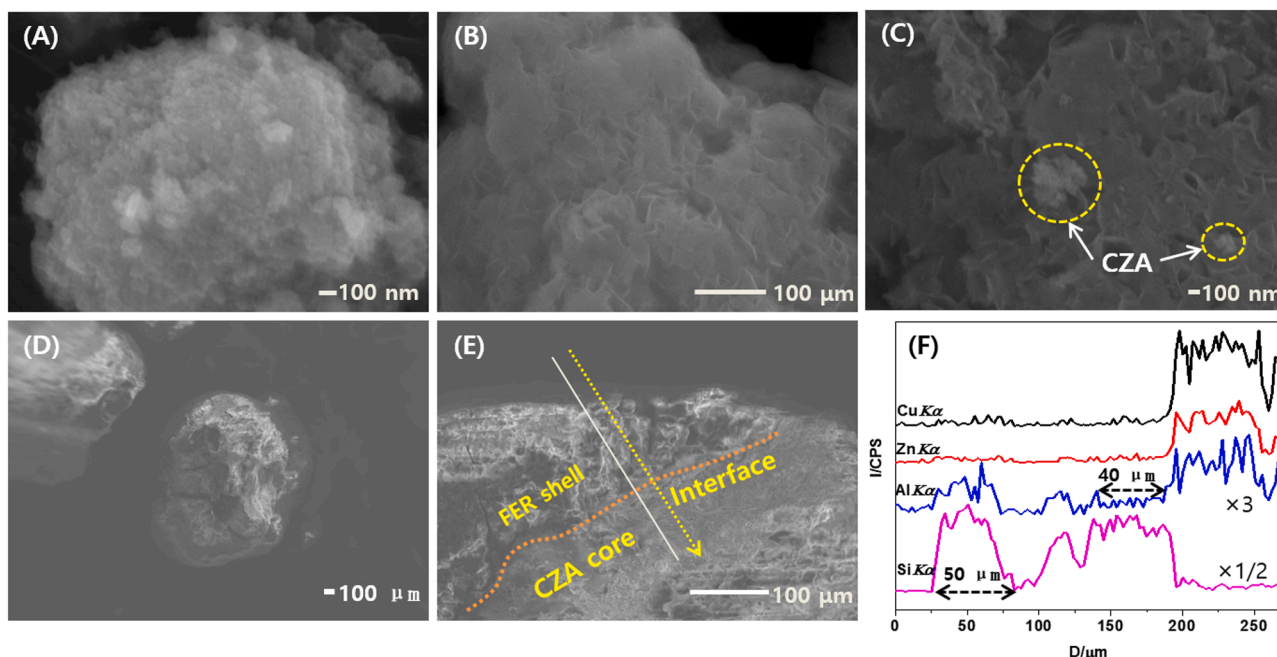


Fig. 2. SEM images of the fresh (A) CZA ($\text{Cu-ZnO-Al}_2\text{O}_3$), (B) ferrierite zeolite (FER), (C) CZA/FER, (D) CZA@FER and (E) and (F) EDS line scanning results of CZA@FER.

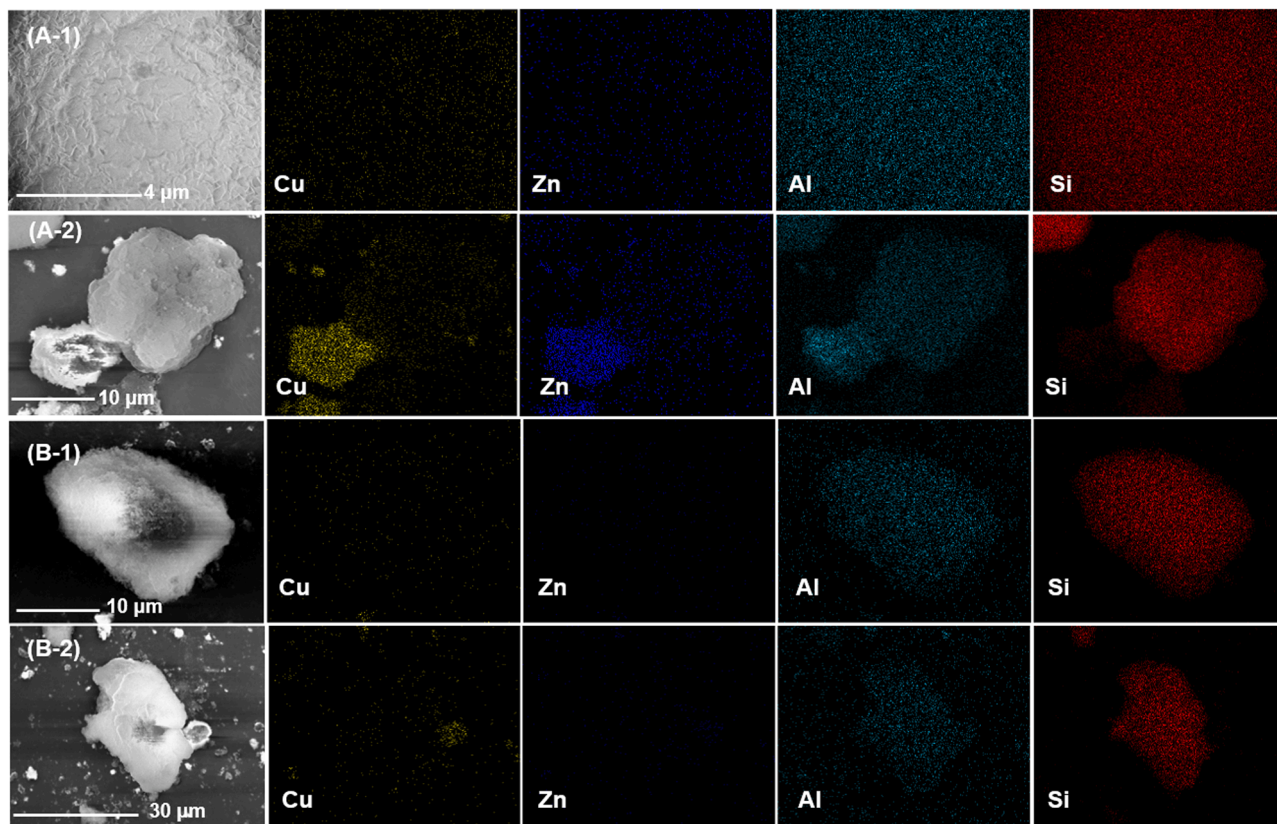


Fig. 3. SEM-EDX mapping images of the (1) fresh and (2) used bifunctional catalysts; (A) CZA/FER and (B) CZA@FER.

displayed in Figs. 3(B-1) and 3(B-2), the smaller surface concentrations of those migrated Cu and Zn metals on the used CZA@FER clearly revealed the suppressed Cu/Zn metal ions migrations with the help of the protective SiO_2 interlayers with their micrometer-scale proximity, which can enhance the durability of the surface acidic sites of the FER

zeolite responsible for the dehydration activity of methanol intermediate to form DME for the present tandem reaction. To further confirm the possible migrations of Cu and Zn metal ions from CZA component to FER zeolite, XPS analysis of Cu 2p and Zn 2p peak on the hybridized CZA/-FER and CZA@FER catalysts after reaction for 40 h was carried out by

compared their BEs with the reference Cu-FER and Zn-FER, and the results are displayed in [supplementary Fig. S3](#). As shown in [Fig. S3\(A\)](#) and [S3\(B\)](#), the much larger peak intensity of Cu 2p and Zn 2p with their lower BEs on the used CZA/FER (932.2 eV for Cu 2p and 1021.5 eV for Zn 2p peak) compared to the used CZA@FER (933.5 eV for Cu 2p and 1022.2 eV for Zn 2p peak) were mainly attributed to the possible migrations of Cu and Zn metal ions with their much stronger interactions on the FER surfaces, especially on the physically mixed CZA/FER. We believe that the facile migrations of Cu and Zn metal ions on the CZA/FER seem to largely change the surface acidic sites by enhancing the catalyst deactivation rate during the present tandem reaction for the direct CO₂ hydrogenation to DME.

3.2. Surface properties of the CZA/FER and CZA@FER catalyst

The reducibility of CuO nanoparticles on the fresh bifunctional catalysts was measured by H₂-TPR and the TPR patterns are displayed in [Fig. 4\(A\)](#). Two characteristic reduction peaks were clearly observed at ~280 and ~340 °C, which can be assigned to the α and β peak for the reduction of Cu²⁺ (CuO phase) and strongly interacted CuO nanoparticles to metallic Cu⁰ species, respectively [31]. The positions of the first reduction α peak were found to be similar at ~285 °C on all the bifunctional catalysts, which were attributed to the highly dispersed CuO nanoparticles in the Cu-ZnO-Al₂O₃ matrices. However, the relatively different interactions of the strongly interacted CuO nanoparticles (β peak) were decreased from 352 °C on the CZA and 345 °C on the

CZA/FER to 338 °C on the CZA@FER, which suggests that the larger CuO nanoparticles on the CZA@FER (confirmed by XRD analysis) can be relatively easily reduced due to their weaker interactions with the FER surfaces with the presence of SiO₂ interlayers. As summarized in [Table 1](#), the amount of H₂ consumption assigned to the α peak was decreased with simultaneous increase of the β peak from 5.40 and 0.54 mmol/g on the CZA, 4.26 and 0.44 mmol/g on the CZA/FER and 3.97 and 1.47 mmol/g on the CZA@FER, respectively. The observation suggests that the thermally stable CuO nanoparticles with their relatively easier reduction natures in the Cu-ZnO-Al₂O₃ matrices can be realized on the SiO₂ interlayer-coated CZA@FER due to the preferential formations of relatively larger CuO nanoparticles as well as weaker interactions between CZA and FER with smaller migration of metal ions to the FER surfaces, which are eventually responsible for an enhanced catalytic performance as well as suppressed deactivation. As displayed in [Fig. 4 \(B\)](#) and summarized in [Table 1](#), the basic sites measured by CO₂-TPD revealed three different desorption peaks at ~130, 400 and 650 °C, assigned to weak (W), medium (M) and strong (S) basic sites, respectively [32,33]. The much smaller CO₂ adsorption capacity (smaller strong basic sites) with the value of 0.27 mmol/g on the CZA@FER compared to that of 1.04–1.18 mmol/g on the CZA and CZA/FER can be also attributed to the SiO₂ interlayer coatings on the basic Cu-ZnO surfaces in the much bigger Cu-ZnO-Al₂O₃ particles, which can further alter the dissociation natures of CO₂ molecules to form oxygenates or CO by RWGS reaction [15].

The acid properties on the fresh and used bifunctional catalysts were

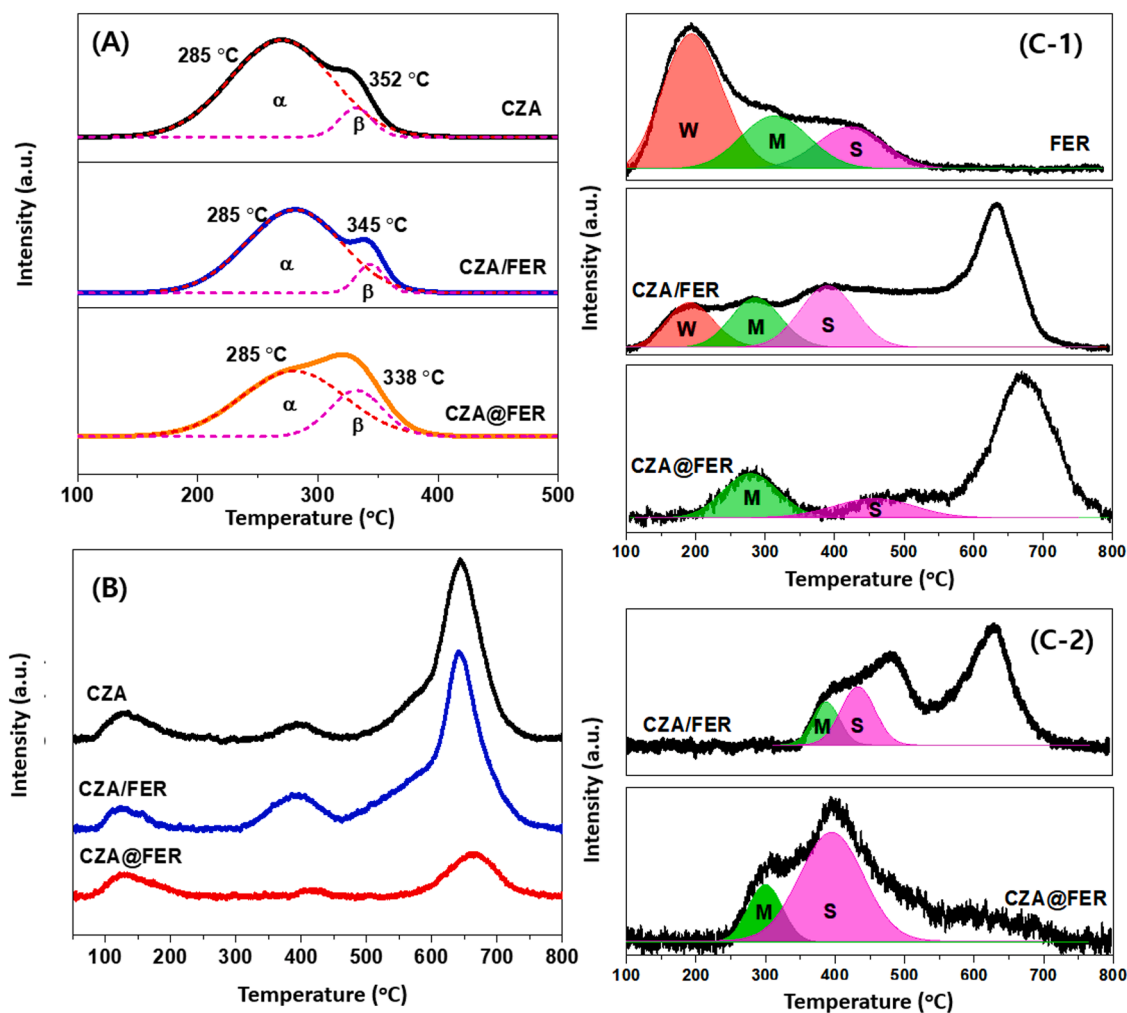


Fig. 4. Surface properties of the fresh bifunctional catalysts; (A) TPR profiles, (B) CO₂-TPD patterns and (C) NH₃-TPD profiles for (1) fresh and (2) used CZA/FER and CZA@FER.

analyzed by NH_3 -TPD and the desorption profiles are displayed in Fig. 4 (C). Based on the NH_3 -TPD profiles on the fresh pristine FER zeolite (Fig. 4(C-1)), three characteristic desorption peaks such as weak (W, below 300 °C), medium (M, 300 – 400 °C) and strong (S, above 400 °C) acidic sites were clearly observed [34,35] with their respective amount of 0.407, 0.131 and 0.166 mmol/g as summarized in supplementary Table S2. With the further incorporation of FER zeolite on the CZA/FER and CZA@FER, the weak acidic sites were largely decreased down to 0.157 and 0 mmol/g (Table 1), respectively, which were attributed to the selective adsorptions of CZA metal ions on the CZA/FER surfaces as well as that of SiO_2 interlayers on the CZA@FER. The observed larger desorption peak above 500 °C on the bifunctional catalysts can be possibly originated by water desorption from the hydroxy groups on the Cu-ZnO- Al_2O_3 lattices or FER surfaces [33–35] or from Lewis acidic sites on the copper surfaces [36]. Interestingly, the total amount of medium and strong acidic sites with 0.400 mmol/g was found to be much larger on the CZA/FER compared to the FER itself with 0.297 mmol/g, which can be attributed to the possible migrations of CZA metal ions on the FER surfaces during the physical powder-mixing step by forming more defected acidic sites on the FER or Cu-ZnO- Al_2O_3 surfaces. Therefore, the acidic sites were largely suppressed on the SiO_2 interlayer-coated CZA@FER with the value of 0.081 mmol/g (supplementary Table S2). In addition, those acidic site distributions were more clearly observed on the used CZA/FER and CZA@FER as shown in Fig. 4(C-2) and supplementary Table S2, where those weak acidic sites on the CZA/FER were not found due to their complete blockages by the migrated Cu/Zn metal ions with small amount of medium and strong acidic sites with 0.026 and 0.044 mmol/g, respectively. However, the stable preservation of

those medium and strong acidic sites on the used CZA@FER was found with the respective value of 0.016 and 0.057 mmol/g due to the suppressed migrations of Cu/Zn metal ions with the help of thicker SiO_2 interlayers.

Those migrations of Cu/Zn metal ions seem to suppress total acidic sites as well as increase the much stronger acidic sites, which can cause much faster deactivation for dehydration rate originated from the metal ions migrations during the reaction by forming lots of undesired products as well [22,23]. For the successive tandem reaction of the direct CO_2 hydrogenation to DME on the bifunctional CZA-FER catalysts, the Cu, Zn or Al metal ions on the Cu-ZnO- Al_2O_3 hydrogenation catalyst can be preferentially migrated on the FER surfaces due to the excessively formed water during CO_2 hydrogenation, which was more dominant on the CZA/FER with the natures of their nanometer-scale proximity. Those metal ions migrations can further decrease the acidic sites by exchange the protons on the FER surfaces as confirmed by NH_3 -TPD results, which eventually decrease the rate of DME formation on the closely interconnected CZA/FER catalyst. In addition, the migrated Cu or Zn species on the zeolites can act as more active sites for RWGS reaction to form CO selectively [22,37,38], which was responsible for an increased CO selectivity during the cascade reaction. However, the stable preservation of medium and strong acidic sites on the CZA@FER seems to be responsible for an enhanced catalytic activity (dehydration of methanol to DME on the surface acidic sites) and stability due to the suppressed migrations of those metal ions through the SiO_2 interlayers with ~ 40 μm thickness between the Cu-ZnO- Al_2O_3 and FER zeolite. In addition, the core-shell structured CZA@FER can also enhance the DME formation rate through the confined spaces between the Cu-ZnO- Al_2O_3 and FER by

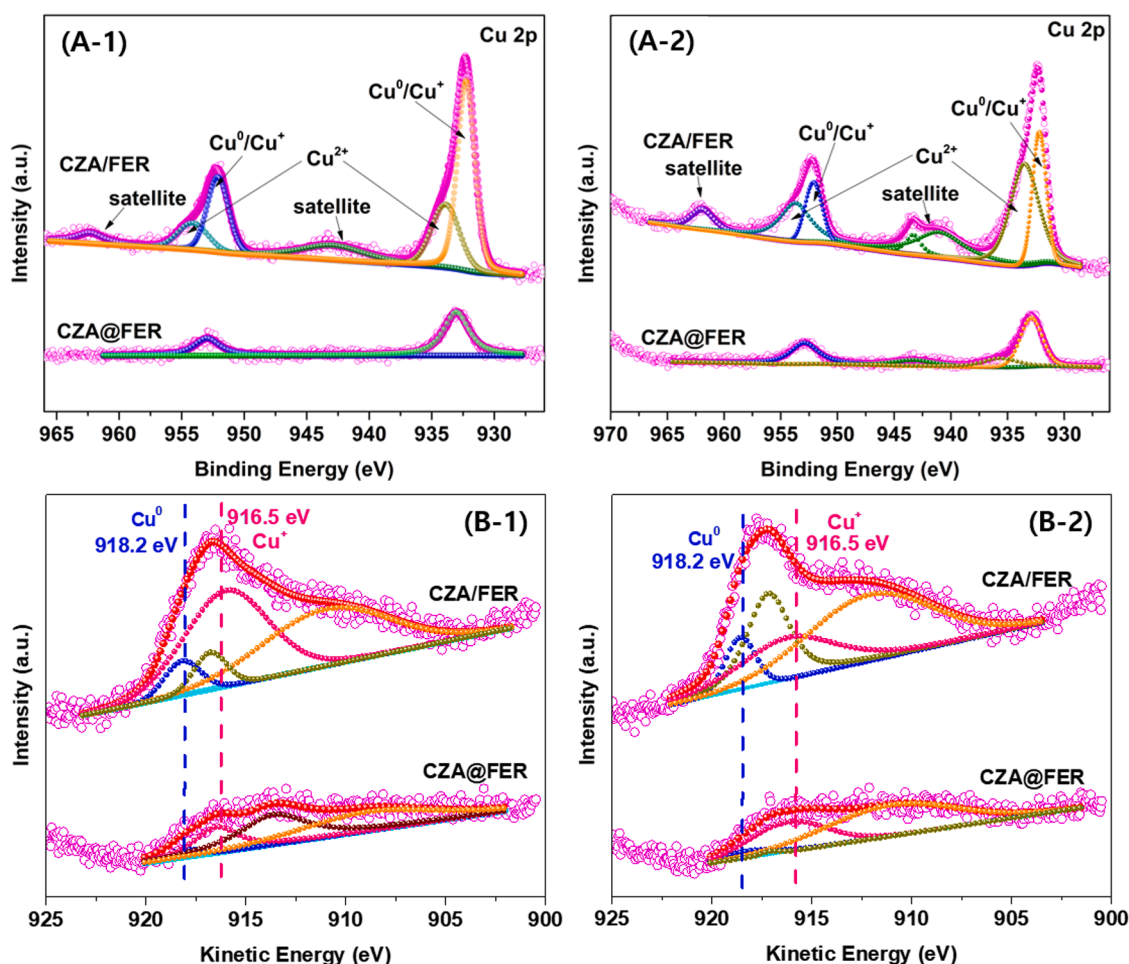


Fig. 5. (A) XPS spectra and (B) AES spectra of the (1) reduced and (2) used bifunctional catalysts (CZA/FER and CZA@FER).

adjusting the diffusion rate of methanol intermediate, which was not observed on the open-structured and physically powder-mixed CZA/FER.

The outermost surface oxidation states of Cu nanoparticles as well as its surface contents were measured by XPS and AES analysis on the reduced and used CZA/FER and CZA@FER, and the results are displayed in Fig. 5 and summarized in Table 1 and supplementary Table S3. On the reduced CZA/FER (Fig. 5(A-1)), the metallic Cu^0 and partially oxidized Cu^+ species were preferentially found with smaller amount of Cu^{2+} (CuO) species, while no apparent peak assigned to Cu^{2+} species was observed on the reduced CZA@FER which suggests that the open-structured CZA/FER can be more easily oxidized with the help of water formed by CO_2 hydrogenation [39,40] compared to SiO_2 interlayer-coated CZA@FER. On the used CZA/FER (Fig. 5(A-2)), the Cu^{2+} species was remarkably increased due to the more facile oxidation natures of metallic Cu nanoparticles on the open-structured Cu-ZnO- Al_2O_3 matrices with a higher $\text{Cu}^{2+}/(\text{Cu}^0 + \text{Cu}^+)$ ratio of 2.28. However, an insignificant Cu^{2+} species was formed on the used CZA@FER with the smaller $\text{Cu}^{2+}/(\text{Cu}^0 + \text{Cu}^+)$ ratio of 0.13, which suggest that the metallic Cu species was more stably preserved on the CZA@FER due to the less migrations of metal ions as well as easy water diffusion through the more hydrophobic SiO_2 interlayers as well as ZnO moiety on the Cu-ZnO- Al_2O_3 structures [6,35]. The more dominant hydrophobic surface ZnO moiety on the reduced and used CZA@FER was also confirmed by its smaller Cu/Zn ratio with the respective value of 1.08 and 0.83, which were smaller than those of 1.41 and 1.21 on the reduced and used CZA/FER from the XPS analysis. Therefore, it is worth to note that the more intimate nanometer-scaled proximity on the physically powder-mixed CZA/FER catalyst is more sensitive for deactivation by water formed during the tandem reaction due to its easier adsorption natures resulted in enhancing the migrations of metal ions and easier oxidation natures of Cu nanoparticles as well. However, the SiO_2 interlayer-coated core-shell structured CZA@FER catalyst is more stable due to the isolated CZA and FER component by the SiO_2 interlayers with its proper thickness of $\sim 40 \text{ nm}$, which can suppress the reoxidation of Cu nanoparticles as well as migrations of metal ions by preserving the more hydrophobic acidic sites with the help of larger ZnO moiety on the Cu-ZnO- Al_2O_3 structures.

To further verify the changes of oxidation states of surface Cu nanoparticles on the CZA-FER catalysts, the AES analysis was carried out by comparing the relative $\text{Cu}^+ / (\text{Cu}^0 + \text{Cu}^+)$ ratio on the reduced and used CZA/FER and CZA@FER, and their results are summarized in Table 1 (Table S3) and displayed in Fig. 5(B). The well-known redox active sites of Cu^0 and Cu^+ were more stably preserved on the CZA@FER compared to CZA/FER, where the characteristic AES peaks appeared at 918.2, 916.5 and 917.0 eV are separately assigned to Cu^0 , Cu^+ and Cu^{2+} species [41–43]. The ratio of $\text{Cu}^+ / (\text{Cu}^0 + \text{Cu}^+)$ on the CZA/FER was decreased from 0.87 to 0.73 during the tandem reaction, while its very similar ratios in the range of 0.84 – 0.88 were observed on the CZA@FER. The observation suggests that the appropriate micrometer-scaled proximity between the CZA and FER with the SiO_2 coating interlayers seems to be crucial for an enhanced catalytic activity and stability by preserving the stable redox properties of Cu nanoparticles. On the CZA@FER, the SiO_2 interlayers with $\sim 40 \text{ nm}$ in thickness not only generate an appreciate micrometer-scaled proximity between the Cu-ZnO- Al_2O_3 and FER zeolite but also suppress the migrations of metal ions by preserving the active acidic sites of FER zeolite with the formation of more hydrophobic ZnO-rich surfaces as confirmed by XPS and AES results. Therefore, we tried to further confirm the effects of two different proximities of the CZA/FER and CZA@FER for deriving the best catalyst packing configurations and an excellent catalytic activity and selectivity to desired products in the following section.

3.3. Effects of proximity on catalytic activity, stability and product distribution

The effects of proximity between the Cu-ZnO- Al_2O_3 and FER zeolite for the tandem reaction of CO_2 hydrogenation to methanol on the CZA surfaces and its successive dehydration to DME on the solid acid FER surfaces were further verified by using the physically powder-mixed CZA/FER(PM) and physically coated CZA@FER(PC), and two CO_2 conversions at maximum and steady state as well as product distribution at steady state with time on stream at $T = 260^\circ\text{C}$, $P = 5.0 \text{ MPa}$ and molar ratio of H_2/CO_2 reactants = 3 (equilibrium conversion of $\text{CO}_2 < 25\%$) are displayed in Fig. 6 as well as supplementary Fig. S4 and summarized in Table 2. On the CZA/FER(PM) (Fig. 6(A)), a gradual decrease of CO_2 conversion (18.7% at a steady-state from its initial conversion of 25.2% with a higher deactivation rate (R_D) of 0.17%/h) and lower DME selectivity of 43.2% (inversely increase of methanol selectivity to 6.7%) with time on stream for 40 h were observed, which can be attributed to the incompatibility of the nanometer-scaled proximity of the CZA and FER component due to the easier reoxidation of metallic Cu nanoparticles by water formed by CO_2 hydrogenation as well as due to the facile deactivation of FER surfaces originated from the migrations of metal ions with their much closer proximity. The intimate proximity of CZA and FER component for direct tandem reaction of CO_2 hydrogenation to DME ($2\text{CO}_2 + 6\text{H}_2 \rightarrow \text{CH}_3\text{OCH}_3 + 3\text{H}_2\text{O}$) caused easy accumulations of water molecules on the CZA surfaces, which can accelerate gradual decreases of active redox copper phases (Cu^+/Cu^0) as well as Brønsted acid sites due to losses of active Cu-ZnO metal oxides with its aggregations and migrations to FER surfaces by decreasing CO_2 conversion and DME selectivity. In case of the powder-mixed CZA/FER (PM) compared to the physically coated CZA@FER(PC), water can be much easily accumulated on the active redox copper phases on the Cu-ZnO by oxidizing to more inactive Cu^{2+} phases (as confirmed by XPS/AES analysis shown in Fig. 5 and supplementary Table S3) as well as on the acidic sites of the FER surfaces (as confirmed by NH_3 -TPD analysis shown in Fig. 4) due to the intimate proximity with facile migrations of metal ions, which caused large decrease of DME selectivity with time on stream with smaller decrease of CO_2 conversion as shown in Fig. 6(A) and supplementary Fig. S4. However, more stable CO_2 conversion (23.1% at a steady-state from its initial conversion of 24.6%) and DME selectivity with time on stream on the SiO_2 -interlayers-coated CZA@FER(PC) (Fig. 6(B)) were observed with the much higher DME selectivity of 54.4% (DME formation rate of (R_{DME}) 8.7 mmol/(g·h)) with a lower deactivation rate (R_D) of 0.05%/h. In addition, the SiO_2 interlayer-coated CZA@FER(PC) with micrometer-scaled proximity revealed much lower selectivity to CO (38.8%) formed by RWGS reaction compared to that of CZA/FER(PM) with 50.0%, which can be attributed to the suppressed migrations of the Cu-ZnO metal ions on the FER surfaces to suppress the formation of defected ion-exchanged surfaces on the core-shell structured and hydrophobic CZA@FER(PC) due to the SiO_2 interlayers and excess ZnO moiety in the Cu-ZnO- Al_2O_3 matrices. In addition, water accumulation on the active Cu-ZnO sites on the CZA@FER(PC) seems to be highly suppressed due to the effective isolations of the active Cu-ZnO sites by SiO_2 interlayer, which were also responsible for less oxidation of active redox copper phases (Cu^+/Cu^0) as well as less migration of metal ions by enhancing catalytic stability with more stable DME selectivity (Fig. S4).

Those proximity-dependent catalytic activities were further verified by using the different catalyst packing configurations with various proximity such as granule-mixed CZA/FER(GM, millimeter-scaled proximity) and dual-bed stacking configuration of the CZA/FER(DB, centimeter-scaled proximity). The CZA/FER(GM) as displayed in Fig. 6 (C) showed a steady decrease of CO_2 conversion (18.9% at a steady state) and DME selectivity (52.2%) with a higher deactivation rate of 0.13%/h, which was found to be very similar with the results observed on the CZA/FER(PM). As verified by the SEM-EDS images shown in Figs. S5(A) and 5(C), the facile Zn migration on the FER surfaces was

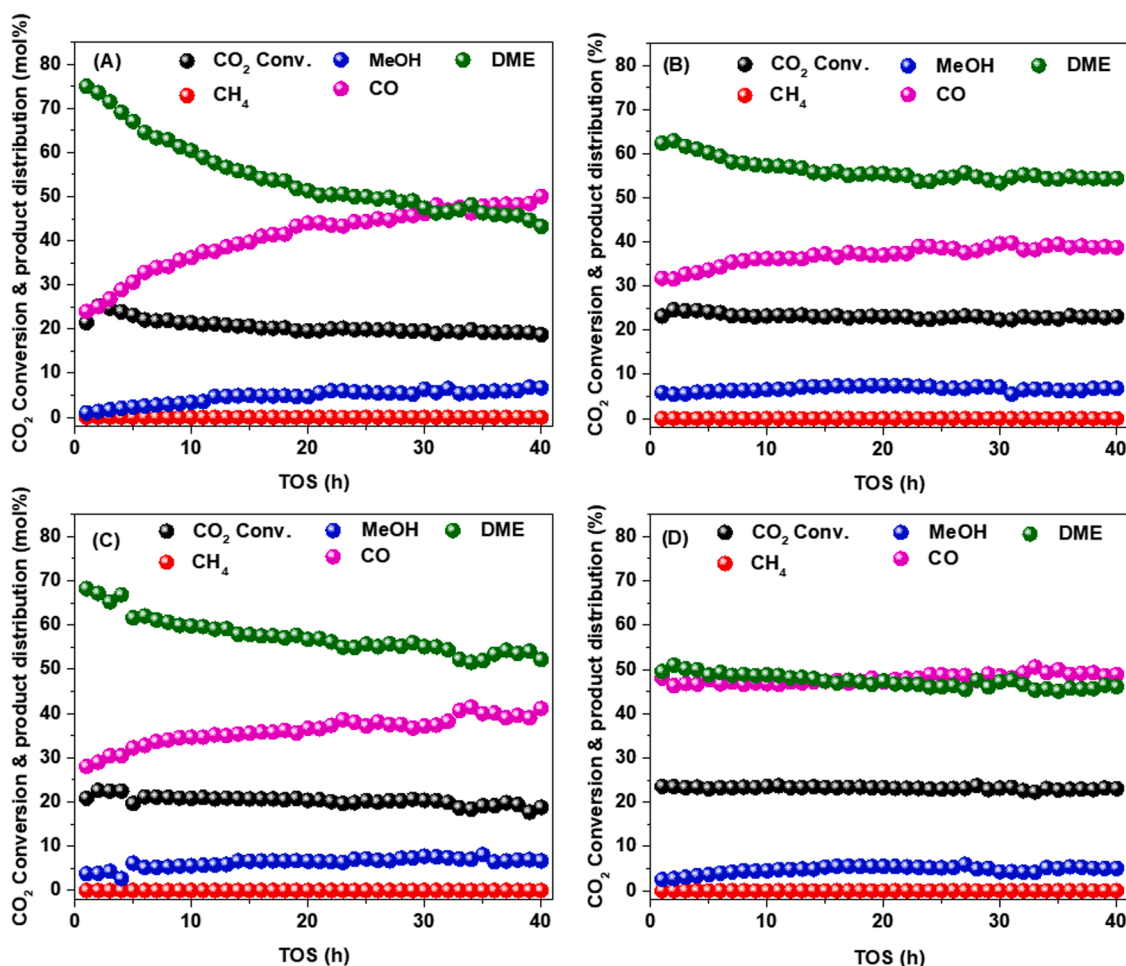


Fig. 6. CO₂ conversion and product distributions (mol%) with time on stream (h) on the bifunctional catalysts with their different proximity; (A) CZA/FER(PM), (B) CZA@FER(PC), (C) CZA/FER(GM) and (D) CZA/FER(DB) catalytic system.

Table 2

Catalytic activity and stability on the bifunctional CZA-FER catalysts according to the proximity of CZA and FER zeolite.

Catalyst proximity ^a	CO ₂ conversion (M ^a x/SS) (mol%)	Selectivity (%)				R _{DME} ^b (mmol/g _{cat} ·h)	R _D ^c (%/h)
		CO	CH ₄	Methanol	DME		
CZA/FER(PM)	25.2/18.7	50.0	0.1	6.7	43.2	6.1	0.17
CZA@FER(PC)	24.6/23.1	38.8	0	6.8	54.4	8.7	0.05
CZA/FER(GM)	22.5/18.9	41.1	0	6.7	52.2	6.9	0.13
CZA/FER(DB)	23.6/23.1	48.8	0.1	5.0	46.1	7.8	0.03
CZA	24.6/23.4	32.9	0	67.1	0	0	0.06

^aCatalytic activity on the bifunctional CZA-FER catalysts (pre-reduced at 300 °C for 5 h with 5% H₂/N₂) was measured for 40 h at the reaction conditions of T = 260 °C, P = 5.0 MPa, H₂/CO₂ = 3 (with 4% N₂ as an internal standard gas) and weight hourly space velocity (SV) = 5000 mL/(g_{cat}·h). The selectivity was represented with steady state values with two CO₂ conversions at maximum (Max) and steady state (SS). The bifunctional CZA-FER catalysts were denoted as the CZA/FER(PM), CZA@FER(PC), CZA/FER(GM) and CZA/FER(DB) for the physical powder mixing(PM), Physical coating(PC), Granule mixing(GM) and Dual-bed(DM) configuration with their different proximity.

^bDME formation rate (R_{DME}, mmol/(g_{cat}·h)) was calculated by using the steady-state value after 35 h on stream.

^cDeactivation rate (R_D, %/h) was calculated by using the difference between maximum and final CO₂ conversion divided by total reaction duration.

observed on the used CZA/FER(GM) with the amount of 0.38 wt%, which suggests that the direct contact between CZA and FER granules can induce the metal ions migrations, especially for Zn species, resulted in its gradual deactivation during the tandem reaction. Although the granule-mixed CZA/FER(GM) showed a slower decrease of CO₂ conversion than that of the CZA/FER(PM), the close interactions between the active Cu-ZnO species and FER surfaces enhanced migrations of metal ions by deactivating surface acidic sites with gradual decrease of DME selectivity with time on stream as shown in Fig. 6(C) and supplementary Fig. S4. Therefore, the much more extended proximity without

direct CZA and FER contact was investigated by using the typical dual-bed configuration on the CZA/FER (DB) and the results are displayed in Fig. 6(D). The more stable CO₂ conversion with time on stream (23.1% at a steady-state) and stable DME selectivity (46.1%) were observed with a little higher CO selectivity of 48.8% and lower deactivation rate of 0.03%/h, which were mainly attributed to the suppressed water accumulations on the Cu-ZnO surfaces with its less reoxidation and migrations to FER surfaces due to no physical contacts between CZA and FER component. Based on the SEM-EDS images as shown in supplementary Fig. S5(B) and S5(D), there were no significant Cu and Zn

migrations on the FER surfaces on the used CZA/FER(DB), which was responsible for its enhanced stability as similar with the SiO₂ interlayer-coated CZA@FER(PC). Based on those different proximity of the CZA and FER zeolite, the much simpler and efficient catalyst configuration of the CZA-FER for the present tandem reaction of the more stable and active direct CO₂ hydrogenation to DME can be simply realized by using the SiO₂ interlayer-isolated CZA@FER(PC) catalytic system. The CZA@FER(PC) catalytic system was found to be more efficient to suppress the migrations of metal ions to the active FER surfaces as well as to prohibit the reoxidation natures of metallic Cu nanoparticles by water formed due to the more hydrophobic surface natures with the ZnO-rich surface moiety on the SiO₂ interlayer-coated Cu-ZnO-Al₂O₃ matrices.

As displayed in Fig. 7(A), the proximity-dependent catalytic configurations with CZA and FER component for the present tandem reaction of direct CO₂ hydrogenation to DME revealed the largely different catalytic activity and product distributions. Compared to the physically powder or granule-mixed CZA/FER(PM) and CZA/FER(GM), the suppressed migrations of metal ions to the FER surfaces and prohibited reoxidation of metallic Cu nanoparticles were realized on the SiO₂ interlayer-coated CZA@FER(PC) with a micrometer-scaled proximity, which were responsible for an enhanced CO₂ conversion and stable product distributions with minimized formation of undesired CO product by RWGS reaction. As summarized in Fig. 7(B), DME selectivity was increased from 43.2% to 52.2% (decrease of CO selectivity from 50.0% to 41.1% inversely) at similar CO₂ conversions of 18.7 – 18.9% with an increase of two active site distance from nanometer CZA/FER(PM) to millimeter CZA/FER(GM), which were attributed to the less migrations of metal ions from Cu-ZnO-Al₂O₃ matrices to FER surfaces due to the longer diffusion distance (millimeter-scaled proximity) as displayed in

Fig. 7(A). Interestingly, the CZA@FER(PC) isolated with the SiO₂ interlayers between the CZA and FER component revealed the much higher CO₂ conversion with 23.1% and DME selectivity of 54.4% with much lower CO selectivity of 38.8% and smaller deactivation rate of 0.05%/h, where the typical dual-bed CZA/FER(DB) also revealed an excellent and similar catalytic activity as well. In addition, the larger amount of FER zeolite also increased the CO selectivity from 39.0 on the CZA@FER (10:1) to 47.6% on the CZA@FER(10:3) with decreased methanol selectivity (from 21.9% to 7.6%) by the further dehydration of methanol and possible reforming reaction of DME on the active FER surfaces as summarized in [supplementary Table S4](#). Therefore, the isolated micrometer-scaled proximity without direct contacts of two active sites on the CZA@FER(PC) are recommended to get a stable activity and product distribution from the beginning of the tandem reaction, which were attributed to the suppressed migrations of metal ions with less reoxidation natures of Cu nanoparticles form the more hydrophobic ZnO moiety on the Cu-ZnO-Al₂O₃ matrices. The schematic diagrams of catalyst deactivation of the bifunctional CZA/FER catalysts are briefly displayed in [supplementary Fig. S6](#). The main reasons for the fast decreases of CO₂ conversion and DME selectivity were attributed to the aggregations of active Cu-ZnO nanoparticles with their reoxidation under water environment and migrations of metal ions to FER surfaces by blocking the active Brønsted acid sites for dehydration reaction. The different migrations and reoxidations of the Cu-ZnO nanoparticles on the FER surfaces were observed according to their different proximity, where the more stable activity was observed on the physically-coated CZA@FER(PC) with similar stability on the completely isolated dual-bed CZA/FER(DB). A close proximity with nanometer-scale on the CZA/FER(PM) accelerated the migration of Cu-ZnO metal ions on the

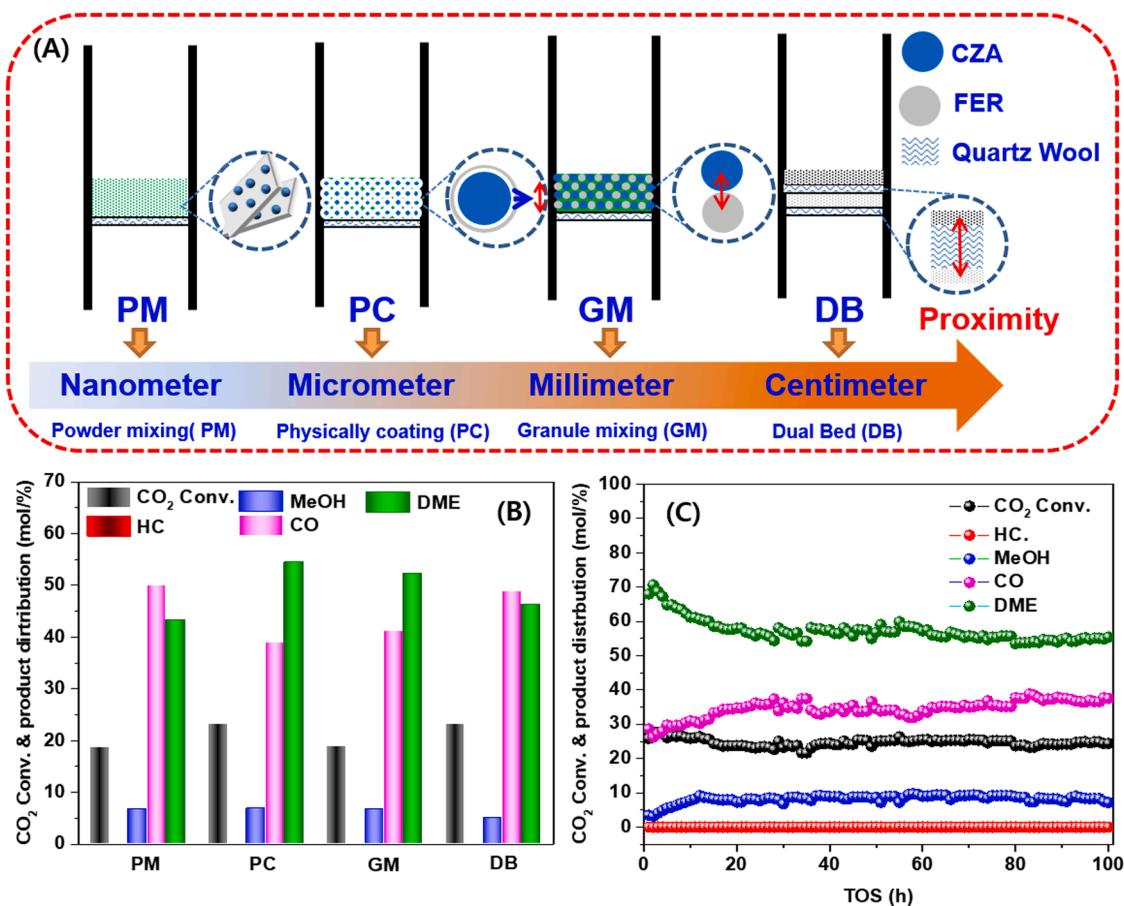


Fig. 7. (A) Schematic diagrams of different proximity-derived bifunctional CZA-FER with CZA/FER(PM), CZA@FER(PC), CZA/FER(GM) and CZA/FER(DB) configuration, (B) Product distributions and (C) Long-term stability of the CZA@FER(PC).

FER surfaces, which largely increased the losses of CO₂ conversion and DME selectivity as shown in [supplementary Fig. S6\(A\)](#), which was properly adjusted by simply introducing SiO₂ coating interlayers on the CZA@FER(PC) as shown in [Fig. S6\(B\)](#). In general, the reduced copper species (Cu⁺/Cu⁰) promoted by ZnO can be easily re-oxidized by the formed water, and the oxidized Cu and Zn species such as Cu(OH)⁺ [44, 45], Cu⁺ [46], Cu²⁺ [47], Zn(OH)⁺ cations [48,49] can be easily migrated to zeolite surfaces to deactivate zeolites by solid state ion-exchange reaction. Those migrations were not properly prevented even with much longer distances between CZA and FER zeolites as revealed by the CZA/FER(GM) as shown in [Fig. S6\(C\)](#), which showed similar catalytic activity with the CZA/FER(PM). However, the complete isolations of CZA and FER on the CZA/FER(DB) also suppressed the migrations with lower deactivation rate as shown in [Fig. S6\(D\)](#), which was realized by introducing the simple SiO₂ interlayer coating method on the CZA@FER(PC).

The closer interactions between the Cu-ZnO-Al₂O₃ and FER zeolite with micrometer-scaled proximity are beneficial to enhance the catalytic activity and stability of the tandem reaction, however, those two catalytically active sites are recommended to be spatially isolated by using the SiO₂ interlayers, which can be better and simple catalyst configuration to realize the dual-bed catalytic system. To further verify the long-term catalytic stability on the optimized CZA@FER(PC), CO₂ conversion and product distributions were measured for 100 h on stream and the activity variations with time on stream are displayed in [Fig. 7\(C\)](#) and the results are summarized in [supplementary Table S5](#). Up to the initial 20 h reaction on time, catalytic activity and product distributions approached to the stabilized values and the catalytic performances were stabilized for the remaining 100 h on stream with smaller deactivation rate of 0.045%/h. CO₂ conversion was stabilized at ~25% with DME selectivity of ~55% and CO selectivity of ~35%, which suggests that the core-shell structured CZA@FER(PC) catalyst with the SiO₂ interlayers can effectively stabilize the acidic sites on the FER zeolite by preventing metal ions migrations from the relatively hydrophobic Cu-ZnO-Al₂O₃ structures as well as by prohibiting the reoxidation of the surface Cu nanoparticles by water formed.

4. Conclusions

Direct synthesis of DME by CO₂ hydrogenation on the bifunctional Cu-ZnO-Al₂O₃ @FER zeolite through typical tandem reaction was investigated in terms of their proximity and the SiO₂ interlayer coating effects. The efficient ways to stabilize the bifunctional catalytic activity and stability were realized by simply using the core-shell structured catalytic configuration of Cu-ZnO-Al₂O₃(CZA) with FER zeolite through the physically coating method with the SiO₂ interlayers (CZA@FER(PC)). The intimate nanometer-scaled proximity between the CZA and FER component on the physically power-mixed CZA/FER(PM) was found to form the detrimental and undesired surface properties through ion-exchange of the FER surfaces with the relatively volatile metal ions migrations from the Cu-ZnO-Al₂O₃, which were responsible for an increased CO selectivity and fast deactivation as well. Those negative FER surface modifications were effectively suppressed by simply introducing SiO₂ interlayers by isolating CZA and FER component, which suppressed the migrations of metal ions to FER surfaces as well as decreased the reoxidation natures of Cu nanoparticles in the more surface ZnO-rich hydrophobic Cu-ZnO-Al₂O₃ matrices.

Declaration of Competing Interest

The authors declare that they have no known competing financial interests or personal relationships that could have appeared to influence the work reported in this paper.

Data availability

No data was used for the research described in the article.

Acknowledgments

The authors also would like to sincerely acknowledge the financial support from the National Research Foundation of Korea (NRF) grant funded by the Korea government (NRF- 2021R1A4A1024129 and NRF-2018M3D3A1A01018009).

Appendix A. Supporting information

Supplementary data associated with this article can be found in the online version at [doi:10.1016/j.apcatb.2023.122456](https://doi.org/10.1016/j.apcatb.2023.122456).

References

- [1] E. Catizzzone, G. Bonura, M. Migliori, F. Frusteri, G. Giordano, CO₂ recycling to dimethyl ether: state-of-the-art and perspectives, *Molecules* 23 (2018) 31.
- [2] K. Saravanan, H. Ham, N. Tsubaki, J.W. Bae, Recent progress for direct synthesis of dimethyl ether from syngas on the heterogeneous bifunctional hybrid catalysts, *Appl. Catal. B: Environ.* 217 (2017) 494–522.
- [3] H. Ham, S.W. Baek, C.H. Shin, J.W. Bae, Roles of structural promoters for direct CO₂ hydrogenation to dimethyl ether over ordered mesoporous bifunctional Cu/M-Al₂O₃ (M = Ga or Zn), *ACS Catal.* 9 (2018) 679–690.
- [4] P.S. Murthy, W. Liang, Y. Jiang, J. Huang, Cu-based nanocatalysts for CO₂ hydrogenation to methanol, *Energy Fuels* 35 (2021) 8558–8584.
- [5] A. Álvarez, A. Bansode, A. Urakawa, A.V. Bavykina, T.A. Wezendonk, M. Makkee, J. Gascon, F. Kapteijn, Challenges in the greener production of formates/formic acid, methanol, and DME by heterogeneously catalyzed CO₂ hydrogenation processes, *Chem. Rev.* 117 (2017) 9804–9838.
- [6] H.S. Jung, F. Zafar, X. Wang, T.X. Nguyen, C.H. Hong, Y.G. Hur, J.W. Choung, M. J. Park, J.W. Bae, Morphology effects of ferrierite on bifunctional Cu-ZnO-Al₂O₃/ferrierite for direct syngas conversion to dimethyl ether, *ACS Catal.* 11 (2021) 14210–14223.
- [7] Y. Zhang, Q. Sun, J. Deng, D. Wu, S. Chen, A high activity Cu/ZnO/Al₂O₃ catalyst for methanol synthesis: preparation and catalytic properties, *Appl. Catal. A: Gen.* 158 (1997) 105–120.
- [8] E.L. Kunkes, F. Stedt, F. Abild-Pedersen, R. Schlögl, M. Behrens, Hydrogenation of CO₂ to methanol and CO on Cu/ZnO/Al₂O₃: is there a common intermediate or not? *J. Catal.* 328 (2015) 43–48.
- [9] E. Catizzzone, A. Aloise, M. Migliori, G. Giordano, Dimethyl ether synthesis via methanol dehydration: effect of zeolite structure, *Appl. Catal. A: Gen.* 502 (2015) 215–220.
- [10] G. Bonura, F. Frusteri, C. Cannilla, G.D. Ferrante, A. Aloise, E. Catizzzone, M. Migliori, G. Giordano, Catalytic features of CuZnZr-zeolite hybrid systems for the direct CO₂-to-DME hydrogenation reaction, *Catal. Today* 277 (2016) 48–54.
- [11] G. Bonura, M. Cordaro, C. Cannilla, A. Mezzapica, L. Spadaro, F. Arena, F. Frusteri, Catalytic behaviour of a bifunctional system for the one step synthesis of DME by CO₂ hydrogenation, *Catal. Today* 228 (2014) 51–57.
- [12] X. An, Y.Z. Zuo, Q. Zhang, D.Z. Wang, J.F. Wang, Dimethyl ether synthesis from CO₂ hydrogenation on a CuO–ZnO–Al₂O₃–ZrO₂/HZSM-5 bifunctional catalyst, *Ind. Eng. Chem. Res.* 47 (2008) 6547–6554.
- [13] A. García-Trenco, A. Martínez, A rational strategy for preparing Cu–ZnO/H-ZSM-5 hybrid catalysts with enhanced stability during the one-step conversion of syngas to dimethyl ether (DME), *Appl. Catal. A: Gen.* 493 (2015) 40–49.
- [14] P.B. Weisz, Polyfunctional heterogeneous catalysis, *Adv. Catal.* 13 (1962) 137–190.
- [15] J. Zecevic, G. Vanbutsele, K.P. de Jong, J.A. Martens, Nanoscale intimacy in bifunctional catalysts for selective conversion of hydrocarbons, *Nature* 528 (2015) 245–248.
- [16] F. Jiao, J. Li, X. Pan, J. Xiao, H. Li, H. Ma, M. Wei, Y. Pan, Z. Zhou, M. Li, S. Miao, J. Li, Y. Zhu, D. Xiao, T. He, J. Yang, F. Qi, Q. Fu, X. Bao, Selective conversion of syngas to light olefins, *Science* 351 (2016) 1065–1068.
- [17] K. Cheng, B. Gu, X. Liu, J. Kang, Q. Zhang, Y. Wang, Direct and highly selective conversion of synthesis gas into lower olefins: design of a bifunctional catalyst combining methanol synthesis and carbon–carbon coupling, *Angew. Chem. Int. Ed.* 128 (2016) 4803–4806.
- [18] P. Gao, S. Li, X. Bu, S. Dang, Z. Liu, H. Wang, L. Zhong, M. Qiu, C. Yang, J. Cai, W. Wei, Y. Sun, Direct conversion of CO₂ into liquid fuels with high selectivity over a bifunctional catalyst, *Nat. Chem.* 9 (2017) 1019–1024.
- [19] J. Wei, Q. Ge, R. Yao, Z. Wen, C. Fang, L. Guo, H. Xu, J. Sun, Directly converting CO₂ into a gasoline fuel, *Nat. Commun.* 8 (2017) 15174.
- [20] Y. Ni, Z. Chen, Y. Fu, Y. Liu, W. Zhu, Z. Liu, Selective conversion of CO₂ and H₂ into aromatics, *Nat. Commun.* 9 (2018) 3457.
- [21] H. Jiang, Z. Hou, Y. Luo, A kinetic view on proximity-dependent selectivity of carbon dioxide reduction on bifunctional catalysts, *ACS Catal.* 10 (2020) 13518–13523.

- [22] Y. Wang, G. Wang, L.I. van der Wal, K. Cheng, Q. Zhang, K.P. de Jong, Y. Wang, Visualizing element migration over bifunctional metal-zeolite catalysts and its impact on catalysis, *Angew. Chem. Int. Ed.* 60 (2021) 17735–17743.
- [23] Y. Ding, F. Jiao, X. Pan, Y. Ji, M. Li, R. Si, Y. Pan, G. Hou, X. Bao, Effects of proximity-dependent metal migration on bifunctional composites catalyzed syngas to olefins, *ACS Catal.* 11 (2021) 9729–9737.
- [24] J.L. Weber, N.A. Krans, J.P. Hofmann, E.J.M. Hensen, J. Zecevic, P.E. de Jongh, K. P. de Jong, Effect of proximity and support material on deactivation of bifunctional catalysts for the conversion of synthesis gas to olefins and aromatics, *Catal. Today* 342 (2020) 161–166.
- [25] F. Frusteri, M. Migliori, C. Cannilla, L. Frusteri, E. Catizzzone, A. Aloise, G. Giordano, G. Bonura, Direct CO₂-to-DME hydrogenation reaction: New evidences of a superior behaviour of FER-based hybrid systems to obtain high DME yield, *J. CO₂ Util.* 18 (2017) 353–361.
- [26] G. Bonura, M. Migliori, L. Frusteri, C. Cannilla, E. Catizzzone, G. Giordano, F. Frusteri, Acidity control of zeolite functionality on activity and stability of hybrid catalysts during DME production via CO₂ hydrogenation, *J. CO₂ Util.* 24 (2018) 398–406.
- [27] V.V. Ordonsky, M. Cai, V. Sushkevich, S. Moldovan, O. Ersen, C. Lancelot, V. Valtchev, A.Y. Khodakov, The role of external acid sites of ZSM-5 in deactivation of hybrid CuZnAl/ZSM-5 catalyst for direct dimethyl ether synthesis from syngas, *Appl. Catal. A: Gen.* 486 (2014) 266–275.
- [28] R. Phienluphon, K. Pinkaew, G. Yang, J. Li, Q. Wei, Y. Yoneyama, T. Vitidsant, N. Tsubaki, Designing core (Cu/ZnO/Al₂O₃)-shell (SAPO-11) zeolite capsule catalyst with a facile physical way for dimethyl ether direct synthesis from syngas, *Chem. Eng. J.* 270 (2015) 605–611.
- [29] G. Bonura, C. Cannilla, L. Frusteri, F. Frusteri, The influence of different promoter oxides on the functionality of hybrid CuZn-ferrierite systems for the production of DME from CO₂-H₂ mixtures, *Appl. Catal. A: Gen.* 544 (2017) 21–29.
- [30] S. Lee, A. Sardesai, Liquid phase methanol and dimethyl ether synthesis from syngas, *Top. Catal.* 32 (2005) 197–207.
- [31] U. Ash-Kurlander, O. Martin, L.D. Fontana, V.R. Patil, M. Bernegger, C. Mondelli, J. Pérez-Ramírez, A. Steinfeld, Impact of daily startup-shutdown conditions on the production of solar methanol over a commercial Cu-ZnO-Al₂O₃ catalyst, *Energy Technol.* 4 (2016) 565–572.
- [32] G. Zhou, Z. He, X. Dong, Role of metal oxides in Cu-based catalysts with NaBH₄ reduction for the synthesis of methanol from CO₂/H₂, *Catal. Lett.* 151 (2021) 1091–1101.
- [33] P.S. Prasad, J.W. Bae, S.H. Kang, Y.J. Lee, K.W. Jun, Single-step synthesis of DME from syngas on Cu-ZnO-Al₂O₃/zeolite bifunctional catalysts: the superiority of ferrierite over the other zeolites, *Fuel Process. Technol.* 89 (2008) 1281–1286.
- [34] X. Feng, P. Zhang, Y. Fang, W. Charusiri, J. Yao, X. Gao, Q. Wei, P. Reubroycharoen, T. Vitidsant, Y. Yoneyama, G. Yang, N. Tsubaki, Designing a hierarchical nanosheet ZSM-35 zeolite to realize more efficient ethanol synthesis from dimethyl ether and syngas, *Catal. Today* 343 (2020) 206–214.
- [35] H. Ham, N.T. Xuan, H.S. Jung, J. Kim, H.S. Roh, J.W. Bae, Crucial factors to maximize DME productivity on hydrophobic bifunctional Cu-ZnO-Al₂O₃/ferrierite by direct CO₂ hydrogenation, *Catal. Today* 369 (2021) 112–122.
- [36] K. Kubo, H. Iida, S. Namba, A. Igarashi, Ultra-high steaming stability of Cu-ZSM-5 zeolite as naphtha cracking catalyst to produce light olefin, *Catal. Commun.* 29 (2012) 162–165.
- [37] D. Vovchok, C. Zhang, S. Hwang, L. Jiao, F. Zhang, Z. Liu, S.D. Senanayake, J. A. Rodriguez, Deciphering dynamic structural and mechanistic complexity in Cu/CeO₂/ZSM-5 catalysts for the reverse water-gas shift reaction, *ACS Catal.* 10 (2020) 10216–10228.
- [38] D. Vovchok, J. Tata, I. Orozco, F. Zhang, R.M. Palomino, W. Xu, L. Harper, S. J. Khatib, J.A. Rodriguez, S.D. Senanayake, Location and chemical speciation of Cu in ZSM-5 during the water-gas shift reaction, *Catal. Today* 323 (2019) 216–224.
- [39] B. Liang, J. Ma, X. Su, C. Yang, H. Duan, H. Zhou, S. Deng, L. Li, Y. Huang, Investigation on deactivation of Cu/ZnO/Al₂O₃ catalyst for CO₂ hydrogenation to methanol, *Ind. Eng. Chem. Res.* 58 (2019) 9030–9037.
- [40] D. Xu, H. Yang, X. Hong, G. Liu, S.C. Edman, Tsang, Tandem catalysis of direct CO₂ hydrogenation to higher alcohols, *ACS Catal.* 11 (2021) 8978–8984.
- [41] Y. Hu, Y. Zhang, J. Du, C. Li, K. Wang, L. Liu, X. Yu, K. Wang, N. Liu, The influence of composition on the functionality of hybrid CuO-ZnO-Al₂O₃/HZSM-5 for the synthesis of DME from CO₂ hydrogenation, *RSC Adv.* 8 (2018) 30387–30395.
- [42] Y. Zhang, D. Li, Y. Zhang, Y. Cao, S. Zhang, K. Wang, F. Ding, J. Wu, V-modified CuO-ZnO-ZrO₂/HZSM-5 catalyst for efficient direct synthesis of DME from CO₂ hydrogenation, *Catal. Commun.* 55 (2014) 49–52.
- [43] P. Gao, F. Li, F. Xiao, N. Zhao, N. Sun, W. Wei, L. Zhong, Y. Sun, Preparation and activity of Cu/Zn/Al/Zr catalysts via hydrotalcite-containing precursors for methanol synthesis from CO₂ hydrogenation, *Catal. Sci. Technol.* 2 (2012) 1447–1454.
- [44] A. Godiksen, P.N. Vennestrom, S.B. Rasmussen, S. Mossin, Identification and quantification of copper sites in zeolites by electron paramagnetic resonance spectroscopy, *Top. Catal.* 60 (2017) 13–29.
- [45] W.M. Ames, S.C. Larsen, DFT calculations of EPR parameters for copper (II)-exchanged zeolites using cluster models, *J. Phys. Chem. A* 114 (2010) 589–594.
- [46] G.T. Palomino, S. Bordiga, C. Lamberti, A. Zecchina, C.O. Arean, Vibrational and optical spectroscopic studies on copper-exchanged ferrierite, *Stud. Surf. Sci. Catal.* 142 (2002) 199–206.
- [47] P. Vanelderen, J. Vancauwenbergh, B.F. Sels, R.A. Schoonheydt, Coordination chemistry and reactivity of copper in zeolites, *Coord. Chem. Rev.* 257 (2013) 483–494.
- [48] I. Pinilla-Herrero, E. Borfecchia, J. Holzinger, U.V. Mentzel, F. Joensen, K. A. Lomachenko, S. Bordiga, C. Lamberti, G. Berlier, U. Olsbye, S. Svelle, J. Skibsted, P. Beato, High Zn/Al ratios enhance dehydrogenation vs hydrogen transfer reactions of Zn-ZSM-5 catalytic systems in methanol conversion to aromatics, *J. Catal.* 362 (2018) 146–163.
- [49] X. Niu, J. Gao, Q. Miao, M. Dong, G. Wang, W. Fan, Z. Qin, J. Wang, Influence of preparation method on the performance of Zn-containing HZSM-5 catalysts in methanol-to-aromatics, *Micropor. Mesopor. Mater.* 197 (2014) 252–261.